A Mixed Nodal-Mesh Formulation for Efficient Extraction and Passive Reduced-Order Modeling of 3D Interconnects

Nuno Marques[+] Mattan Kamon[*] Jacob White[*] L. Miguel Silveira[+]

[+] INESC/Cadence European Laboratories
Dept. of Elect. and Comp. Eng.
Instituto Superior Técnico
1000 Lisboa, Portugal

[*] Research Laboratory of Electronics
Dept. of Elect. Eng. and Comp. Science
Massachusetts Institute of Technology
Cambridge, MA 02139

Abstract

As VLSI circuit speeds have increased, reliable chip and system design can no longer be performed without accurate three-dimensional interconnect models. In this paper, we describe an integral equation approach to modeling the impedance of interconnect structures accounting for both the charge accumulation on the surface of conductors and the current traveling in their interior. Our formulation, based on a combination of nodal and mesh analysis, has the required properties to be combined with Model Order Reduction techniques to generate accurate and guaranteed passive low order interconnect models for efficient inclusion in standard circuit simulators. Furthermore, the formulation is shown to be more flexible and efficient than previously reported methods.

1 Introduction

As VLSI circuit speeds have increased, reliable and accurate chip and system design can no longer be performed without accurate three-dimensional interconnect models. In the past, designers had to cope with tools where 2D models, used for modeling long and uniform interconnect structures, were glued together with 3D models that were necessary for handling discontinuities such as vias through planes, chip-to-board and board-to-board connectors. Not only was this mixing of models cumbersome but, as circuit density continues to increase, such discontinuities become more prevalent. In recent years much effort has been devoted to the study and development of fast and accurate algorithms for computing full 3-D interconnect models directly from Maxwell's equations.

Many of these structures are small compared to a wavelength, and much work has been directed at rapidly solving for the inductance and capacitance of these structures. However inductance and capacitance are not necessarily decoupled quantities, and for higher frequencies a distributed model is necessary. In this paper, we describe an integral equation approach to modeling the impedance of interconnect structures accounting for both the charge accumulation on the surface of conductors and the current traveling along conductors. When high accuracy is desired, the models generated can become excessively large and difficult to solve for a continuous range of frequencies. The need for reduced-size models leads us to consider Model Order Reduction (MOR) techniques, which have been developed in the field of parameter extraction [1, 2, 3, 4, 5, 6, 7, 8, 9].

Our approach, which is based on a combination of nodal analysis formulation with a mesh analysis formulation, has significant advantages over previously reported methods, both in extraction speed and model size, making it possible to generate guaranteed passive low order models for efficient inclusion in a circuit simulator such as SPICE or SPECTRE. Combining our formulation with acceleration techniques such as the Fast Multipole Method [10, 11] or the Precorrected-FFT [12], allows the accurate analysis of larger, more complex three-dimensional geometries than previously possible.

In Section 2 we discuss the integral formulation and discretization from which we derive the circuit equations that describe the interconnect effects. In Section 3 we describe a nodal analysis-based formulation that allows the application of recent model order reduction techniques in order to directly generate passive reduced-order models. We then present an extension to this formulation based on a combination of nodal and mesh analysis that can be used to accelerate model construction. In Section 4 we present results of using the new extraction tool and analyze the performance of the generated reduced-order models. Finally, conclusions are drawn in Section 5.

2 Mathematical Formulation

Parasitic extraction for a set of conductors involves determining the relation between the terminal (or port) currents and the terminal voltages. Given a structure of k terminal pairs, the admittance matrix which relates the terminal currents and the terminal voltages is defined as

$$\boldsymbol{Y}_t(\omega)\boldsymbol{V}_t(\omega) = \boldsymbol{I}_t(\omega), \tag{1}$$

where sinusoidal steady-state at frequency ω is assumed. $\boldsymbol{Y}_t(\omega) \in \mathbb{C}^{k\times k}$, and $\boldsymbol{I}_t, \boldsymbol{V}_t \in \mathbb{C}^k$ are the terminal current and voltage vectors, respectively [13]. If it is possible to compute the currents given the voltages at the terminals then, by adding voltage sources to all terminals in the circuit, $\boldsymbol{Y}_t(\omega)$ can be computed one column at a time. To do this, we set entry i of $\boldsymbol{V}_t$ to one, the others to zero, and solve for $\boldsymbol{I}_t$, which will be the i^{th} column of $\boldsymbol{Y}_t(\omega)$.

To derive a relation between voltages and currents, we resort to an integral equation approach derived directly from Maxwell's equations and similar to the Partial Element Equivalent Circuit (PEEC) method [14]. At each point inside the conductors, we have [15]

$$\boldsymbol{E} = -\nabla\varphi - \frac{\partial \boldsymbol{A}}{\partial t} \tag{2}$$

where

$$\varphi(\boldsymbol{r},t) = \frac{1}{4\pi\epsilon}\int_{V'}\frac{\rho(\boldsymbol{r'})}{\|\boldsymbol{r}-\boldsymbol{r'}\|}dv' \tag{3}$$

$$\boldsymbol{A}(\boldsymbol{r},t) = \frac{\mu}{4\pi}\int_{V'}\frac{\boldsymbol{J}(\boldsymbol{r'})}{\|\boldsymbol{r}-\boldsymbol{r'}\|}dv'. \tag{4}$$

In deriving equations, the Electromagneto-Quasistatic assumption was considered. This approximation corresponds to assuming that the influence of the charge and currents at any point in the structure is instantaneously felt everywhere. That is to say, we consider the speed of light as infinite. So, our model will be valid only for structures small compared to a wavelength. (In practice, however, one can analyze structures on the order of a wavelength, because the interaction terms where retardation time is significant correspond to weak coupling).

DAC 98, June 15-19, 1998, San Francisco, CA USA
ISBN 1-58113-049-x/98/06…$5.00

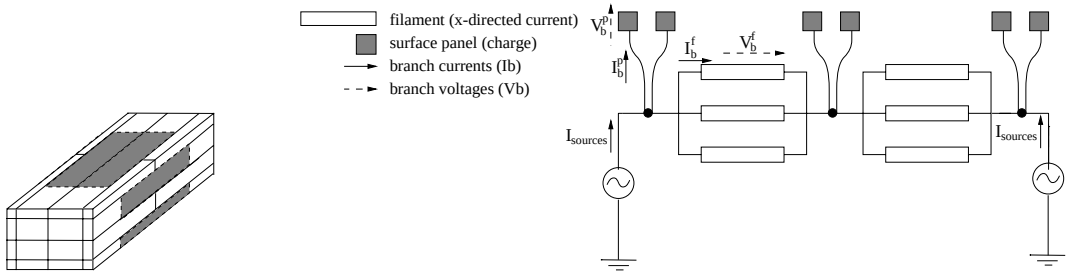

(a) (b)

Fig. 1. a) Results of discretization operation applied to a conductor showing volume filaments (with its cross section decreasing toward the surfaces to properly capture skin and proximity effects) and charge panels (only some panels are shown); b) A simplified version of the correspondent electrical circuit – nodal analysis quantities are described.

To compute a model from this formulation, a discretization operation is performed on the conductors. Following the PEEC approach, the interior of each conductor is divided into a grid of filaments where each filament is assumed to have a constant current density with the direction of its length, and the surfaces of the conductors are covered with panels, where each panel is assumed to have a constant charge density. For conductors that are very long and thin we can assume that the current running along its length is much larger than the current running along the other two orthogonal directions. In those cases, a filament discretization along a single direction is performed. For planar conductors, the filament discretization must be performed along two coordinate directions and for volume-like conductors, filaments are set along the three-coordinate directions. This discretization operation allows us to generate an equivalent electrical "circuit" made up of filaments and panels. Figure 1-a) shows the discretization operation applied to a long and thin conductor (filaments along one direction only) and Figure 1-b) shows the electrical circuit associated with it.

To generate the constitutive relations for these elements, we apply the Galerkin method to (2), after discretizing the equation (see [14] for details). A constitutive relation for the filaments is obtained in the form of

$$\boldsymbol{Z}_L \boldsymbol{I}_b^f \equiv (\boldsymbol{R} + j\omega \boldsymbol{L}) \boldsymbol{I}_b^f = \boldsymbol{V}_b^f \tag{5}$$

where $\boldsymbol{I}_b^f \in \mathbb{C}^f$ is the vector of f filament currents,

$$R_{ii} = \frac{l_i}{\sigma a_i} \tag{6}$$

is the $f \times f$ diagonal matrix of filament DC resistances, and

$$L_{ij} = \frac{\mu}{4\pi a_i a_j} \int_{V_i} \int_{V_j'} \frac{\mathbf{l_i} \cdot \mathbf{l_j}}{\|\boldsymbol{r} - \boldsymbol{r}'\|} dV' \, dV \tag{7}$$

is the $f \times f$ dense, symmetric positive semidefinite matrix of partial inductances. $\boldsymbol{V}_b^f = \boldsymbol{\Phi}_{n_1} - \boldsymbol{\Phi}_{n_2}$ is the vector of voltages given as the difference between the node potentials, $\boldsymbol{\Phi}_n$, at the two ends of the filament.

In our formulation, and unlike the PEEC method, the coefficients of the potential matrix $\boldsymbol{P}$, which relates node potentials to panel charges, are computed such that charge conservation is verified on every node. In our case, for p panels, $\boldsymbol{P} \in \mathbb{R}^{p \times p}$ will be computed as:

$$P_{ij} = \frac{1}{A_j 4\pi\epsilon_0} \int_{p_j'} \frac{1}{\|\boldsymbol{r}_{p_i} - \boldsymbol{r}'\|} dV', \tag{8}$$

that is in the form of partial coefficients of potential - where p_j' is the surface of panel j, A_j its area and $\boldsymbol{r}_{\boldsymbol{p}_i}$ is the center of each panel p_i. Note that we allow multiple panels on each node - as is the case for nodes on edges or apices of conductors. Furthermore, we shall see that this allows us to establish a set of equations amenable to generate passive reduced-order models.

Since the current flowing onto the panels is given by $\boldsymbol{I}_b^p = \frac{d}{dt}\boldsymbol{q}_p$, $\boldsymbol{q}_p \in \mathbb{C}^p$ being the charge on each of the p panels, for the sinusoidal steady state we can write $\boldsymbol{q}_p = \boldsymbol{I}_b^p/(j\omega)$. Additionally, since the panel node voltages are voltages relative to infinity, we can view the panel branches as connecting the panel node to the zero potential node at infinity. Then the panel branch voltages are given by $\boldsymbol{V}_b^p = \boldsymbol{\Phi}_p - 0 = \boldsymbol{\Phi}_p$, where $\boldsymbol{\Phi}_p$ are the panel potentials. Combining, we get a relation between the panel currents and their voltages,

$$\boldsymbol{V}_b^p = \frac{1}{j\omega} \boldsymbol{P} \boldsymbol{I}_b^p \tag{9}$$

With (5) and (9) we can write the constitutive relations for the elements as a single matrix in $\mathbb{C}^{b \times b}$, $b = f + p$,

$$\boldsymbol{V}_b = \begin{bmatrix} \boldsymbol{V}_b^f \\ \boldsymbol{V}_b^p \end{bmatrix} = \begin{bmatrix} \boldsymbol{Z}_L & 0 \\ 0 & \boldsymbol{P}/(j\omega) \end{bmatrix} \begin{bmatrix} \boldsymbol{I}_b^f \\ \boldsymbol{I}_b^p \end{bmatrix} = \boldsymbol{Z} \boldsymbol{I}_b. \tag{10}$$

where $\boldsymbol{I}_b \in \mathbb{R}^b$ is the vector of branch (filaments and panels) currents and $\boldsymbol{V}_b$ is the vector of branch (filaments or panels) voltages. See Figure 1-b) for an illustration of these quantities.

Applying voltage sources to the circuit, we can now solve it, and extract the desired terminal currents, thus producing the required admittance model. To that end we will use a Modified Nodal Analysis technique. Note that only voltage sources can be used because one needs to connect all the sources to the zero potential node at infinity and that node is only connected to capacitors. This is necessary in order to be able to obtain DC results, which are desirable if we want to use the model in time-domain simulations.

Kirchoff's Current Law, which implies that the sum of the branch currents leaving each node in the network must be zero, can be written as

$$\begin{bmatrix} \boldsymbol{A} & -\boldsymbol{N} \end{bmatrix} \begin{bmatrix} \boldsymbol{I}_b \\ \boldsymbol{I}_{src} \end{bmatrix} = \begin{bmatrix} 0 \end{bmatrix} \tag{11}$$

where $\boldsymbol{A} \in \mathbb{R}^{n \times b}$ is the sparse nodal incidence matrix summing the filament and panel currents in each node, $\boldsymbol{N} \in \mathbb{R}^{n \times n_{src}}$ is the sparse matrix summing the currents through the voltage sources, n is the number of nodes (excluding the one for the point at infinity), b is the number of branches (filaments plus panels), and n_{src} is the number of voltage sources in the circuit. $\boldsymbol{I}_{src} \in \mathbb{R}^{n_{src}}$ is the vector of currents leaving each voltage source (always connected to ground) and entering the terminal nodes. Note the 0 in the right hand side due to the absence of current sources in the circuit.

Applying Kirchoff's Voltage Law to the circuit, we obtain

$$\begin{bmatrix} \boldsymbol{A}^T \\ \boldsymbol{N}^T \end{bmatrix} \begin{bmatrix} \boldsymbol{V}_n \end{bmatrix} = \begin{bmatrix} \boldsymbol{V}_b \\ \boldsymbol{V}_{src} \end{bmatrix} \tag{12}$$

where $\boldsymbol{V}_n$ is the vector of voltages at each node in the network, $\boldsymbol{V}_{src}$ are the known source voltages. Note that $\boldsymbol{V}_{src}$ is exactly the terminal voltage vector $\boldsymbol{V}_t$, from (1). Combining (12) with (11) and

(10) yields the system of equations

$$\begin{bmatrix} \boldsymbol{Z} & -\boldsymbol{A}^T & 0 \\ \boldsymbol{A} & 0 & -\boldsymbol{N} \\ 0 & \boldsymbol{N}^T & 0 \end{bmatrix} \begin{bmatrix} \boldsymbol{I}_b \\ \boldsymbol{V}_n \\ \boldsymbol{I}_{src} \end{bmatrix} = \begin{bmatrix} 0 \\ 0 \\ \boldsymbol{V}_{src} \end{bmatrix} \tag{13}$$

One approach to coupling the above models with circuits is to directly include an admittance model, for instance some version of (13), into a circuit simulator. This approach has the drawback that the size of the system in (13) can easily be very large if high-accuracy is desired. Even computing the admittance matrix directly, as described at the beginning of this section is inefficient, as it requires t solutions of a system with a very large matrix. The use of iterative methods could reduce the computational cost of solving this system but the resulting model would be valid only at a single frequency. However to design with this admittance model it is often necessary to perform coupled simulation with nonlinear devices, such as CMOS drivers and receivers. Nonlinear devices require time domain simulation, and thus the admittance information is necessary from DC up to the highest frequency of interest in the circuit. Thus, it is essential to have models valid for a continuous range of frequencies.

3 Guaranteed Passive Model Order Reduction and Interconnect Simulation

Recently, Model Order Reduction (MOR) algorithms [1, 2, 5, 9, 6] have been presented to solve this problem. The basic idea of MOR techniques is to reduce the size of the system described by the circuit equations, usually written in a convenient state-space form, to a much smaller one that still captures the dominant behavior of the original system. This approximation is then used to generate a model amenable to be inserted in a circuit simulator such as SPICE or SPECTRE. The field of MOR has matured significantly in the past few years. Recently, MOR techniques, such as the PRIMA algorithm [6], have been presented, that produce guaranteed stable and passive reduced-order models.

To apply this algorithm, the circuit equations are written in the state-space form

$$\begin{aligned} s\boldsymbol{\mathcal{L}}\,\boldsymbol{x} &= -\boldsymbol{\mathcal{R}}\,\boldsymbol{x} + \boldsymbol{B}\,\boldsymbol{u} \\ \boldsymbol{y} &= \boldsymbol{B}^T\boldsymbol{x}. \end{aligned} \tag{14}$$

where $s = j\omega$. To generate passive reduced order models both $\left(\boldsymbol{\mathcal{R}} + \boldsymbol{\mathcal{R}}^T\right)$ and $\left(\boldsymbol{\mathcal{L}} + \boldsymbol{\mathcal{L}}^T\right)$ must be positive semidefinite. It was shown in [16] that it is possible to derive a state-space form with these properties when Mesh analysis is applied to the circuit. We will now describe how a state-space form with these properties can also be derived using Modified Nodal Analysis.

3-1 Nodal Formulation

To derive a state space form of (13), the powers of the Laplace variable $s = j\omega$ must all be to the first powers only. However, the constitutive relation $\boldsymbol{Z}$ in (10) contains terms with both s and $1/s$. To separate the $1/s$ power, note that as seen in Figure 1-b), the branch currents can be separated into two types, $\boldsymbol{I}_b = [\boldsymbol{I}_b^f; \boldsymbol{I}_b^p]$ where $\boldsymbol{I}_b^f$ represents the currents in filaments and $\boldsymbol{I}_b^p$ represents the currents onto panels. Also, $\boldsymbol{A}$ can be split into $[\boldsymbol{A}_e; \boldsymbol{A}_i]$ where $\boldsymbol{A}_e$ corresponds to the n_e external nodes (an external node is a node that has at least one panel connected to it) and $\boldsymbol{A}_i$ corresponds to the n_i internal nodes (an internal node is a node to which no panels are connected). Based on this categorization, (11) becomes

$$\begin{bmatrix} \boldsymbol{A}_e & \boldsymbol{B}_e & -\boldsymbol{N}_e \\ \boldsymbol{A}_i & 0 & 0 \end{bmatrix} \begin{bmatrix} \boldsymbol{I}_b^f \\ \boldsymbol{I}_b^p \\ \boldsymbol{I}_{src} \end{bmatrix} = \begin{bmatrix} 0 \\ 0 \end{bmatrix}. \tag{15}$$

The zero-blocks in (15) correspond to $\boldsymbol{B}_i$ and $\boldsymbol{N}_i$, which are always null since there are no panels or voltage sources connected to internal nodes. We can also rewrite (12) separating the branch voltages in $\boldsymbol{V}_b = [\boldsymbol{V}_b^f; \boldsymbol{V}_b^p]$. $\boldsymbol{V}_n^e$ and $\boldsymbol{V}_n^i$ correspond to, respectively, the voltage in external and internal nodes:

$$\begin{bmatrix} \boldsymbol{A}_e^T & \boldsymbol{A}_i^T \\ \boldsymbol{B}_e^T & 0 \\ \boldsymbol{N}_e^T & 0 \end{bmatrix} \begin{bmatrix} \boldsymbol{V}_n^e \\ \boldsymbol{V}_n^i \end{bmatrix} = \begin{bmatrix} \boldsymbol{V}_b^f \\ \boldsymbol{V}_b^p \\ \boldsymbol{V}_{src} \end{bmatrix} \tag{16}$$

The desired equation in state-space form can then be obtained using (15) and (16) and the constitutive relations expressed in (10). Using the first equation in (15) and the constitutive relation for the panels, we can write

$$\boldsymbol{A}_e\boldsymbol{I}_b^f + s\boldsymbol{B}_e\boldsymbol{P}^{-1}\boldsymbol{V}_b^p - \boldsymbol{N}_e\boldsymbol{I}_{src} = 0 \tag{17}$$

Furthermore, using the second relation in (16), we have

$$\boldsymbol{A}_e\boldsymbol{I}_b^f + s\boldsymbol{B}_e\boldsymbol{P}^{-1}\boldsymbol{B}_e^T\boldsymbol{V}_n^e - \boldsymbol{N}_e\boldsymbol{I}_{src} = 0 \tag{18}$$

Now using the constitutive relation for filaments with the first relation in (16), yields

$$(\boldsymbol{R} + s\boldsymbol{L})\boldsymbol{I}_b^f - \boldsymbol{A}_e^T\boldsymbol{V}_n^e - \boldsymbol{A}_i^T\boldsymbol{V}_n^i = 0 \tag{19}$$

Finally, using (18) and (19) plus the relations not yet used in (15) and (16), we obtain the desired state-space form:

$$s\begin{bmatrix} \boldsymbol{L} & 0 & 0 & 0 \\ 0 & \boldsymbol{B}_e\boldsymbol{P}^{-1}\boldsymbol{B}_e^T & 0 & 0 \\ 0 & 0 & 0 & 0 \\ 0 & 0 & 0 & 0 \end{bmatrix} \begin{bmatrix} \boldsymbol{I}_b^f \\ \boldsymbol{V}_n^e \\ \boldsymbol{V}_n^i \\ \boldsymbol{I}_{src} \end{bmatrix} = \tag{20}$$

$$-\begin{bmatrix} \boldsymbol{R} & -\boldsymbol{A}_e^T & -\boldsymbol{A}_i^T & 0 \\ \boldsymbol{A}_e & 0 & 0 & -\boldsymbol{N}_e \\ \boldsymbol{A}_i & 0 & 0 & 0 \\ 0 & \boldsymbol{N}_e^T & 0 & 0 \end{bmatrix} \begin{bmatrix} \boldsymbol{I}_b^f \\ \boldsymbol{V}_n^e \\ \boldsymbol{V}_n^i \\ \boldsymbol{I}_{src} \end{bmatrix} + \begin{bmatrix} 0 \\ 0 \\ 0 \\ \boldsymbol{V}_{src} \end{bmatrix}.$$

which can readily be written as (14).

It was shown in [17] that this system has the properties mentioned above as necessary to generate guaranteed passive reduced order models. Model Order Reduction techniques can thus be applied directly to either this formulation or the one developed in [16] using Mesh Analysis. Considering an expansion point at $s = 0$, for which the matrix $\boldsymbol{\mathcal{R}}$ needs to be inverted, the sizes of the resulting reduced-order models produced by those formulations is similar for similar accuracy. However, because the number of states in the nodal formulation is smaller, it is, for most cases, faster to obtain a reduced-order model using this formulation. Indeed, the number of states in the nodal case is

$$f + n + n_{src} \tag{21}$$

where f is the number of filaments, n the number of nodes in the network, and n_{src} is the number of sources; the number of states in the mesh formulation is

$$m + p = f + p - n + 1 \simeq f + 2p - n \tag{22}$$

where m is the total number of meshes and p is the total number of panels. So the nodal formulation is smaller if $p > n$, which is always the case for a discretization along one or two directions.

As described in [18], and as we shall see in the results section, interconnect models derived using the Electromagneto-Quasistatic assumption, which captures skin effect, have in general a large number of real poles that have a weak effect on the system behavior. Many of these poles are near the origin and moment-matching around $s = 0$ tends to match these non-dominant poles first, and only then consider more important outward poles. Thus it might be useful to consider using other expansion points. An obvious choice would be $s = \infty$. For certain structures, it turns out that the size of the reduced models obtained with expansions around $s = \infty$ can be significantly smaller, for similar accuracy, than the sizes of those obtained with expansions around $s = 0$. Therefore, the ability to perform expansions around any point in the complex plane,

including $s = \infty$, is an important property of the nodal formulation. For expansions around $s = \infty$, the matrix $\boldsymbol{\mathcal{L}}$ from (14) will require inversion. Unlike mesh analysis, in the nodal formulation $\boldsymbol{\mathcal{L}}$ is non-singular if there are no internal nodes, a common situation since for most structures discretizing conductors along one direction is sufficient. Note that in order to derive a model based on an expansion around $s = \infty$, one needs to consider current sources, instead of voltage sources, and so the $\boldsymbol{I}_{src}$ unknowns do not appear in the system.

3-2 Mixed Nodal-Mesh Formulation

Computing a reduced-order model from (14) with an algorithm such as PRIMA, using any expansion point, corresponds to solving a linear system with a matrix that involves $\boldsymbol{\mathcal{R}}$ and $\boldsymbol{\mathcal{L}}$ in some form. If $s = 0$ is considered then the system matrix is $\boldsymbol{\mathcal{R}}^{-1}\boldsymbol{\mathcal{L}}$. In the case $s = \infty$ presented above, $\boldsymbol{\mathcal{L}}$ must be inverted directly to form the system matrix (note that $\boldsymbol{\mathcal{L}}$ is never inverted explicitly: if $\boldsymbol{\mathcal{L}}^{-1}\boldsymbol{b} = \boldsymbol{x}$ is needed, $\boldsymbol{\mathcal{L}}\boldsymbol{x} = \boldsymbol{b}$ is solved for $\boldsymbol{x}$ using an iterative algorithm such as GMRES [19]). In any case, the smaller the condition number of $\boldsymbol{\mathcal{L}}$, the faster the convergence will be.

The form of the $\boldsymbol{\mathcal{L}}$ matrix reveals one of the differences between the Nodal and Mesh formulations. In the latter the block matrices describing the filament constitute relations appear together with the mesh matrix $\boldsymbol{M}$, thus the block $\boldsymbol{MLM}^T$ in $\boldsymbol{\mathcal{L}}$, while in the former $\boldsymbol{L}$ is used directly, as shown in (20).

It is known that under an appropriate choice of preconditioner, the condition number of a system obtained from the matrix $\boldsymbol{MLM}^T$ can be *significantly smaller* than that obtained from the partial inductance matrix $\boldsymbol{L}$ (see [20] for a proof). Thus faster system solution using $\boldsymbol{\mathcal{L}}$ can be accomplished in the nodal formulation if the block $\boldsymbol{L}$ were replaced by a term like $\boldsymbol{MLM}^T$ in $\boldsymbol{\mathcal{L}}$, as in the mesh formulation. Such a substitution implies the combination of a mixed nodal and mesh analysis method taking advantage of the best characteristics of each system. Although this mixed nodal-mesh formulation was developed to be combined with PEEC-style discretizations, the authors have been made aware that the resulting approach is quite similar to a specialized basis function methods presented in [21].

Using Mesh Analysis, we know that

$$\boldsymbol{M}\boldsymbol{V}_b = \boldsymbol{V}_s \tag{23}$$

$$\boldsymbol{M}^T\boldsymbol{I}_m = \boldsymbol{I}_b. \tag{24}$$

Eqn. (23) is based on Kirchoff's Voltage Law, which implies that the sum of branch voltages around each mesh in the network must be zero. $\boldsymbol{V}_b$ is the vector of branch voltages, $\boldsymbol{V}_s$ is the mostly zero vector of source voltages and $\boldsymbol{M}$ is the mesh incidence matrix. Eqn. (24), on the other hand, is based on Kirchoff's Current Law, and establishes a relation between the mesh currents $\boldsymbol{I}_m$ and the branch currents $\boldsymbol{I}_b$. Consider now separating the branch terms in (23) and (24) for filaments ($\boldsymbol{V}_b^f, \boldsymbol{I}_b^f$) and panels ($\boldsymbol{V}_b^p, \boldsymbol{I}_b^p$). Three different types of meshes in the circuit are then considered: those that contain only filaments - $\boldsymbol{M}_f$ (with mesh currents $\boldsymbol{I}_m^b$), those that contain only panels - $\boldsymbol{M}_p$ (with mesh currents $\boldsymbol{I}_m^p$), and those that contain both filaments and panels - $\boldsymbol{M}_{fs}, \boldsymbol{M}_{ps}$ (with mesh currents $\boldsymbol{I}_m^s$). Rewriting Eqns. (23) and (24) in terms of these variables leads to

$$\begin{bmatrix} \boldsymbol{M}_f & & \\ & \boldsymbol{M}_p & \\ \boldsymbol{M}_{fs} & \boldsymbol{M}_{ps} & \end{bmatrix} \begin{bmatrix} \boldsymbol{V}_b^f \\ \boldsymbol{V}_b^p \\ \boldsymbol{V}_b^p \end{bmatrix} = \begin{bmatrix} 0 \\ \boldsymbol{V}_s^p \\ 0 \end{bmatrix} \tag{25}$$

$$\begin{bmatrix} \boldsymbol{M}_f^T & & \boldsymbol{M}_{fs}^T \\ & \boldsymbol{M}_p^T & \boldsymbol{M}_{ps}^T \end{bmatrix} \begin{bmatrix} \boldsymbol{I}_m^f \\ \boldsymbol{I}_m^p \\ \boldsymbol{I}_m^s \end{bmatrix} = \begin{bmatrix} \boldsymbol{I}_b^f \\ \boldsymbol{I}_b^p \end{bmatrix} \tag{26}$$

Using the first equation in (26), multiplying the first line of (20) $\boldsymbol{M}^f$, and using $\boldsymbol{I}_m^{f+s}$, where

$$\boldsymbol{M}^f = \begin{bmatrix} \boldsymbol{M}_f \\ \boldsymbol{M}_{fs} \end{bmatrix} \qquad \boldsymbol{I}_m^{f+s} = \begin{bmatrix} \boldsymbol{I}_m^f \\ \boldsymbol{I}_m^s \end{bmatrix}$$

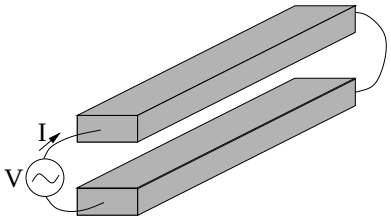

Fig. 3. Example geometry to compare models obtained at various expansion points.

the final state space-form is, then,

$$s\begin{bmatrix} \boldsymbol{M}^f\boldsymbol{L}\boldsymbol{M}^{f\,T} & 0 & 0 & 0 \\ 0 & \boldsymbol{B}_e\boldsymbol{P}^{-1}\boldsymbol{B}_e^T & 0 & 0 \\ 0 & 0 & 0 & 0 \\ 0 & 0 & 0 & 0 \end{bmatrix} \begin{bmatrix} \boldsymbol{I}_m^{f+s} \\ \boldsymbol{V}_n^e \\ \boldsymbol{V}_n^i \\ \boldsymbol{I}_{src} \end{bmatrix} =$$

$$-\begin{bmatrix} \boldsymbol{M}^f\boldsymbol{R}\boldsymbol{M}^{f\,T} & -\boldsymbol{M}^f\boldsymbol{A}_e^T & -\boldsymbol{M}^f\boldsymbol{A}_i^T & 0 \\ \boldsymbol{A}_e\boldsymbol{M}^{f\,T} & 0 & 0 & -\boldsymbol{N}_e \\ \boldsymbol{A}_i\boldsymbol{M}^{f\,T} & 0 & 0 & 0 \\ 0 & \boldsymbol{N}_e^T & 0 & 0 \end{bmatrix} \begin{bmatrix} \boldsymbol{I}_m^{f+s} \\ \boldsymbol{V}_n^e \\ \boldsymbol{V}_n^i \\ \boldsymbol{I}_{src} \end{bmatrix}$$

$$+\begin{bmatrix} 0 \\ 0 \\ 0 \\ \boldsymbol{V}_{src} \end{bmatrix} \tag{27}$$

or, equivalently, adding the output equations

$$\begin{aligned} s\boldsymbol{\mathcal{L}}\,\boldsymbol{x} &= -\boldsymbol{\mathcal{R}}\,\boldsymbol{x} + \boldsymbol{B}\,\boldsymbol{V}_t \\ \boldsymbol{I}_t &= \boldsymbol{B}^T\boldsymbol{x}. \end{aligned} \tag{28}$$

In this mixed formulation, again both the $\boldsymbol{\mathcal{R}}$ and $\boldsymbol{\mathcal{L}}$ matrices satisfy the conditions required for passive MOR. The size of the system is the same as that of the nodal formulation. Also as for nodal, $\boldsymbol{\mathcal{R}}$ and $\boldsymbol{\mathcal{L}}$ (subjected to the same restrictions) are non-singular, meaning that any expansion point can be used in the model order reduction.

4 RESULTS

In this section examples will be considered that allow the study of the efficiency of MOR techniques when applied to the extraction of 3D interconnects using the formulation proposed in this paper. First, models of a simple structure generated using expansion points at $s = 0$ and $s = \infty$ will be explored and compared. Then a model of a connector example, will be analyzed in order to verify the formulation. To attest to the accuracy of the formulation and the reduction algorithms, results of a time-domain analysis of the connector model will be compared with experimental measurements.

4-1 A simple two-conductor example

Consider the simple geometry made up of two long and thin conductors, as shown in Figure 3, whose dominant behavior is similar to a transmission line. Both conductors are $1cm$ long, $37\mu m$ wide, $13\mu m$ in height and the distance between conductors is $17\mu m$. For this example a discretization is chosen such that 416 panels are used to cover all surfaces. Each conductor is divided into 10 segments along its length and each segment is divided into 15 filaments to properly capture skin effect. Figure 2 shows the efficiency of reduced models, compared with the full model, with expansion points at $s = 0$ and $s = \infty$. The full system has 323 states for an expansion point $s = 0$ (voltage sources are used in this case; for $s = \infty$ current sources are used). For this example a 62^{th}-order model was generated. Figure 2-a) and c) show the positioning of the system and reduced-order model poles, for expansions around $s = 0$ and $s = \infty$ respectively, while Figure 2-b) and d) show the magnitude of the frequency dependent impedance of both the full system and the reduced models for each situation. Note that, because we have to use different sources for $s = 0$ and $s = \infty$, the poles in the figure relative to $s = 0$ are the admittance poles, while in that relative to $s = \infty$, they are impedance poles.

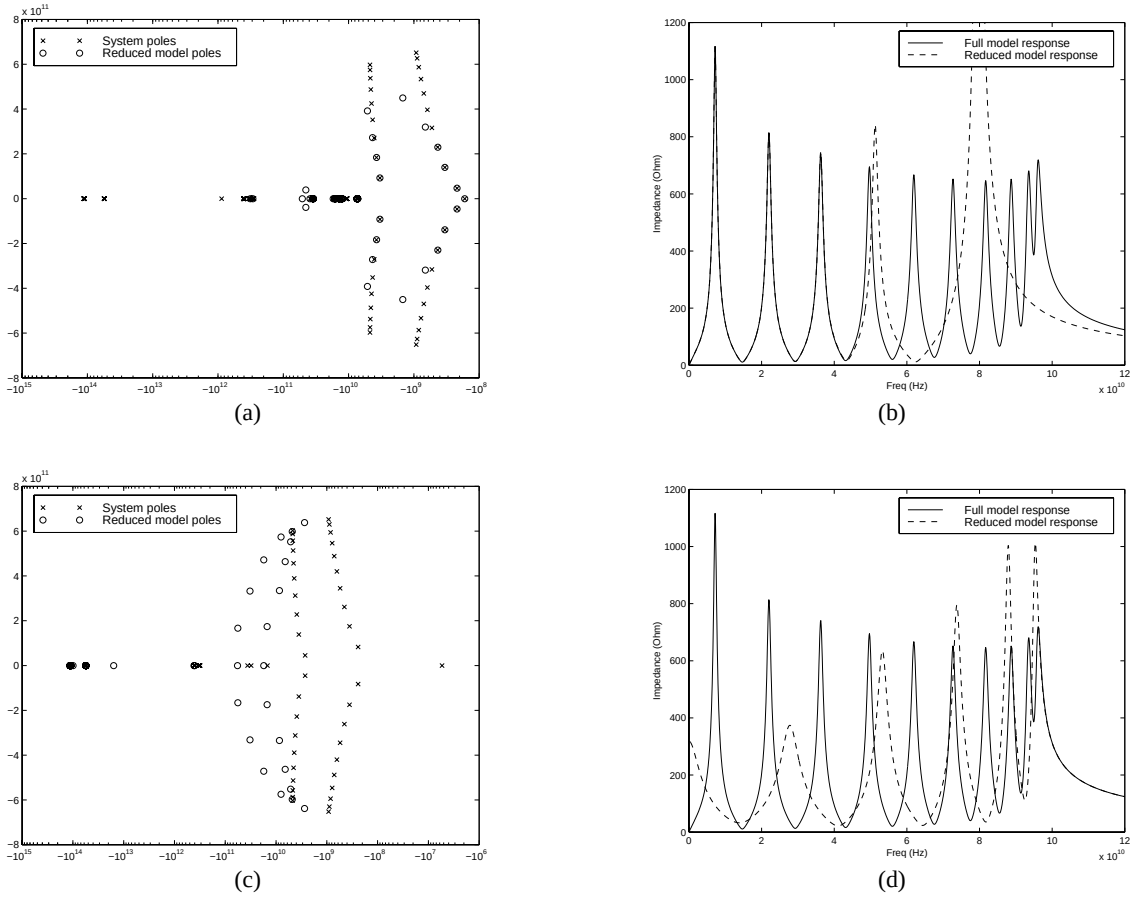

Fig. 2. Results obtained for the example geometry using the nodal-mesh formulation using an expansion point of $s = 0$ ((a) and (b)) and an expansion point of $s = \infty$ ((c) and (d)). In (a) the admittance poles are shown, while in (c) the impedance poles are plotted.

It is important to note the large number of poles of the full system along the real axis. Almost all of these poles have a weak effect on the final response (they have very small residues). For this example we found that only around 15% of the poles are relevant. These poles appear due to the large number of filaments connected in parallel (capacitances in panels are summed in each node, in the formulation, and so do not contribute with weak poles). These non-dominant poles are responsible for the large orders required for the reduced models shown since, for expansions around $s = 0$ or $s = \infty$, there is always a large cluster of such poles "nearby" and the MOR algorithm will capture them. However only about 22 of these poles are necessary to maintain the accuracy of the model as shown in the figures.

This simple geometry demonstrates some of the differences from expanding at different points. For $s = 0$, when the order of the reduced models is increased, we obtain a model that is accurate for an increasingly larger frequency range. However, for $s = \infty$, all the reduced models are inaccurate until full accuracy is suddenly achieved for a specific order, smaller than the original system size. This is because the algorithm, in the $s = \infty$ case, tries to first match all of the weak poles near -10^{14} before matching any of the dominant ones while in the $s = 0$ case the distance between the dominant and the weak poles near zero is smaller.

4-2 Connector example

Figure 4 presents an eighteen-pin portion of a real backplane connector structure. The connector is composed of 18 pins with a ground shield around and between the conductors. A discretization operation is performed using 582 filaments and 864 panels. Figure 5 shows the results obtained for the self-impedance of a single pin using the mixed nodal-mesh formulation with different order reduced models computed using an expansion around $s = 0$. The full system has 658 states. In the figure, models with orders 182 and 420 are compared to the exact response. Similarly to what was found for the first structure presented, only a small number of these poles are relevant, in this case 78 and 110 respectively.

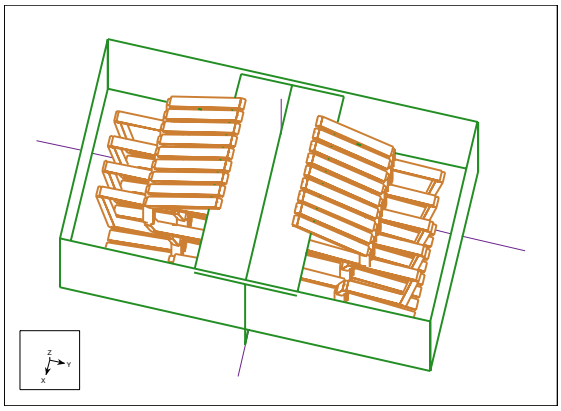

Fig. 4. A 3D connector.

Finally, in Figure 6 we present a comparison between results of a time-domain simulation obtained with a reduced model generated with our formulation and experimental measurements. For this ex-

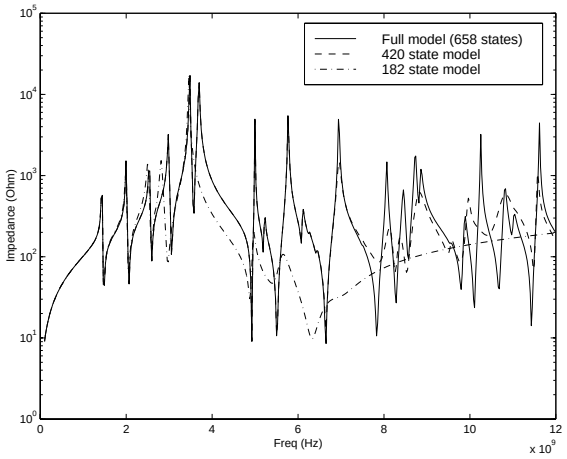

Fig. 5. Various reduced order models for the connector

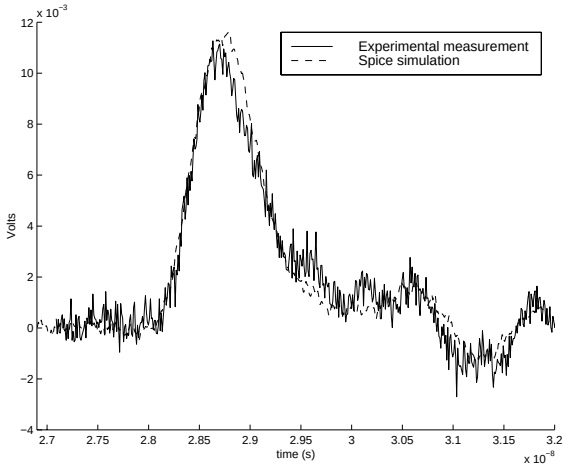

Fig. 6. Comparison between measured time-domain waveforms and simulated results obtained using a reduced-order model of the connector example.

periment all pins are connected to ground through resistors. Then a noisy input is connected in series with one of these resistors and a step with a $500ps$ rise-time is imposed on it. The voltage waveform at an adjacent pin is collected. As can be seen from the plot the waveforms are qualitatively similar and acceptable accuracy is obtained. If higher accuracy is required, a finer discretization can be used.

5 Conclusions

The main contribution of this paper is the presentation of a modeling approach based on a mixed nodal-mesh formulation. This formulation, when combined with recent Model Order Reduction algorithms, allows for the generation of guaranteed passive reduced order models of three-dimensional interconnect structures. The mixed nodal-mesh method takes advantage of the flexibility introduced by the nodal analysis, namely by maintaining relatively small model sizes and the ability to use expansion points at any frequency, and adds to it the good conditioning properties of the mesh analysis matrices. Important properties of the new formulation, such as the ability to use any expansion point in the complex plane, were illustrated with an example. Also, a comparison between measured data and the time-domain response of a generated model of a real 3-D connector structure, was used to validate the accuracy of the formulation. Further research is still required in order to improve the model generation process such that only the set of dominant poles is captured.

Acknowledgments

The authors would like to thank Mike Tsuk of Digital Equipment Corp. for the practical example. This work was partially supported by the National Science Foundation, the Portuguese JNICT programs PRAXIS XXI and FEDER under contracts 2/2.1/T.I.T/1661/95 and 2/2.1/T.I.T/1639/95 and grant BM-8592/96.

References

[1] Lawrence T. Pillage and Ronald A. Rohrer. Asymptotic Waveform Evaluation for Timing Analysis. *IEEE Trans. CAD*, 9(4):352–366, April 1990.

[2] P. Feldmann and R. W. Freund. Efficient linear circuit analysis by Padé approximation via the Lanczos process. *IEEE Trans. on Computer-Aided Design of Integrated Circuits and Systems*, 14:639–649, 1995.

[3] L. Miguel Silveira, Mattan Kamon, and Jacob K. White. Efficient reduced-order modeling of frequency-dependent coupling inductances associated with 3-d interconnect structures. In *Proc. 32^{nd} Design Automation Conf.*, pages 376–380, San Francisco, CA, June 1995.

[4] K. J. Kerns, I. L. Wemple, and A. T. Yang. Stable and efficient reduction of substrate model networks using congruence transforms. In *Int. Conf. on Computer Aided Design*, pages 207 – 214, San Jose, CA, November 1995.

[5] L. Miguel Silveira, Mattan Kamon, Ibrahim Elfadel, and Jacob K. White. A coordinate-transformed Arnoldi algorithm for generating guaranteed stable reduced-order models of rlc circuits. In *Int. Conf. on Computer Aided-Design*, pages 288–294, San Jose, California, November 1996.

[6] Altan Odabasioglu, Mustafa Celik, and Lawrence Pileggi. Prima: Passive reduced-order interconnect macromodeling algorithm. In *Int. Conf. on Computer Aided-Design*, pages 58–65, San Jose, California, November 1997.

[7] I. M. Elfadel and David D. Ling. Zeros and passivity of Arnoldi-reduced-order models for interconnect networks. In *34^{nd} Design Automation Conf.*, pages 28–33, Anaheim, California, June 1997.

[8] I. M. Elfadel and David. L. Ling. A block rational arnoldi algorithm for multipoint passive model-order reduction of multiport rlc networks. In *Int. Conf. on Computer Aided-Design*, pages 66–71, San Jose, California, November 1997.

[9] Eric Grimme. *Krylov Projection Methods for Model Reduction*. PhD thesis, Coordinated-Science Laboratory, University of Illinois at Urbana-Champaign, Urbana-Champaign, IL, 1997.

[10] L. Greengard and V. Rokhlin. A fast algorithm for particle simulations. *Journal of Comp. Physics*, 73(2):325–348, December 1987.

[11] K. Nabors and J. White. Fast capacitance extraction of general three-dimensional structures. *IEEE Trans. on Microwave Theory and Techniques*, June 1992.

[12] J. R. Phillips. Error and complexity analysis for a collocation-grid-projection plus precorrected-FFT algorithm for solving potential integral equations with Laplace or Helmholtz kernels. In *Proc. 1995 Copper Mountain Conf. on Multigrid Methods*, April 1995.

[13] C. Desoer and E. Kuh. *Basic Circuit Theory*. McGraw-Hill, New York, 1969.

[14] Albert E. Ruehli. Equivalent circuit models for three-dimensional multiconductor systems. *IEEE Trans. on Microwave Theory and Techniques*, MTT-22(3):216–221, March 1974.

[15] E. C. Jordan and K. G. Balmain. *Electro-Magnetic Waves and Radiating Systems*. Prentice-Hall, Englewood Cliffs, N.J., 1968.

[16] M. Kamon, N. Marques, and J. White. FastPep: A Fast Parasitic Extraction Program for Complex Three-Dimensional Geometries. In *Int. Conf. on Computer Aided-Design*, San Jose, California, November 1997.

[17] Nuno Marques, Mattan Kamon, Jacob White, and L. Miguel Silveira. An efficient algorithm for fast parasitic extraction and passive order reduction of 3d interconnect models. In *DATE'98 - Design, Automation and Test in Europe, Exhibition and Conference*, pages 538–548, Paris, France, February 1998.

[18] Mattan Kamon, Nuno Marques, L. Miguel Silveira, and Jacob K. White. Generating reduced order models via peec for capturing skin and proximity effects. In *Proc. IEEE 6^{th} Topical Meeting on Electrical Performance of Electronic Packaging, Monterey, CA*, San Jose, California, October 1997.

[19] Y. Saad and M. H. Schultz. GMRES: A generalized minimal residual algorithm for solving nonsymmetric linear systems. *SIAM Journal on Scientific and Statistical Computing*, 7:856–869, July 1986.

[20] Mattan Kamon. Efficient techniques for inductance extraction of complex 3-d geometries. Master's thesis, Massachusetts Institute of Technology, February 1994.

[21] S. M. Rao, D. R. Wilton, and A. W. Glisson. Electromagnetic scattering by surfaces of arbitrary shape. *IEEE Trans. Antennas Propagat.*, AP-30(3):409–418, May 1997.